

Improving Viral Diagnostic Methods: A Plasmonic Nanoparticle Virion Counting and Interpretation System Utilizing MATLAB

Bryan Hong & Jai Pal

Table of Contents

I.	Introduction	3-4
II.	Engineering Goal	4-5
III.	Materials	5
IV.	Synthesis of the 15 nm AuNPs	6
V.	Conjugation of the Antibodies and RSV with the AuNPs	6-8
VI.	Detection System Setup	9-10
VII.	Plasmonic Nanobubble Counting Mechanism	10-12
VIII.	Single Virion Counting Mechanism	12-14
IX.	Results and Conclusions	15-18
X.	Future Research and Applications	18
XI.	Acknowledgements	19
XII.	Work Cited	19-20

I. Introduction

After crippling society for the last two years, the COVID-19 pandemic was an important wake-up call for society, exposing our need for a more effective system in protecting for its citizens against viruses. One major cause of this burden are the flaws in our current diagnostic methods. Both nucleic acid tests and antibody tests have major issues and technologically lag behind our current medical advancements. For example, the nucleic acid test can deliver accurate results with a 97% success rate; however, they take from 24-72 hours for results to be accurately evaluated. The antibody test on the other hand, delivers rapid results in just over 15 minutes; however, they only presented a 75% success rate in correctly diagnosing the patient, according to a study conducted by the University of Massachusetts. Furthermore, our world has realized the urgent need for a more advanced and sophisticated system of diagnosis that allows for more information on the virus sample to be collected during diagnosis. One example of this is viral quantification. Viral load quantification provides scientists with important analytics and insights about the viral load that unlocks our ability to understand things such as the prognosis of a virus and the severity of symptoms. For example, by analyzing cycle thresholds in COVID-19 test results, scientists are able to connect and gather data about infection trends and other critical pieces of information in order to better personalize and design treatments for specific patients. However, our current means of viral quantification involving cycle thresholds create too much variability and aren't standardized enough to be utilized effectively. Today's research experiment uses the Respiratory Syncytial Virus (RSV) as a model target for the virus diagnosis in this experiment, but the system designed today can be calibrated and replicated for other viruses of this sort. Historically, the Human Respiratory Syncytial Virus

(RSV) has been attributed as the major respiratory pathogen in young children and infants.

Figure 1: Etiology of acute respiratory infections in children worldwide

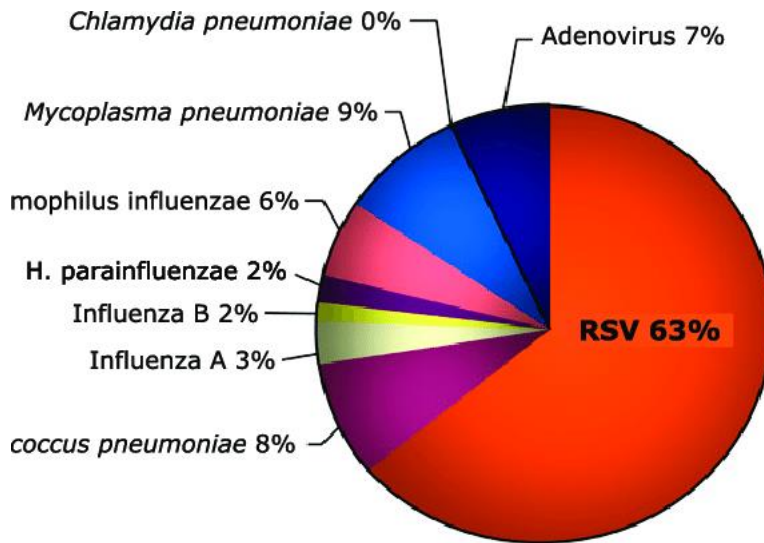


Figure created by Giovanni Piedimonte, 2014

II. Engineering Goal

The primary objective of this project is to create a sensitive Human Respiratory Syncytial Virus (RSV) diagnostic algorithm using a digital plasmonic nanobubble photodetection system that can be replicated and calibrated for diagnosing other viruses such as but not limited to: SARS-COV-2, Influenza A & B, different strains of the Rhinovirus, Human Parainfluenza Viruses, and other types of respiratory viruses. Unlike our current gold standard, the PCR test, this diagnostic method retrieves rapid and accurate results without the need for a virus amplification step, allowing us to save resources and time. Compared to our current technology of antigen rapid test kits, this diagnostic method retrieves results both more rapidly and accurately. Additionally, this project utilizes a MATLAB coding algorithm to conduct a single

virion counting system that allows scientists to identify the severity of the symptoms and predict the prognosis of the RSV sample.

III. Materials

The materials that were utilized to create this project were divided up into three different categories: chemical, biological, and mechanical. The chemical materials that were utilized include: 98 mL of Deionized Water (dH₂O) with a resistivity of 18.2 MΩ·cm, 0.338 mL of 2.23 nm AuNP seeds, 1 mL of 99% 25 mM Tetrachloroauric (III) acid trihydrate (HAuCl₄·3H₂O), 1 mL of 99% 112.2 mM Sodium Citrate tribasic dihydrate (Na₃CA·2H₂O), Sodium Chloride (NaCl), 50 mg of 5 mM 3,3'-Dithiobis (sulfosuccinimidyl propionate) (DTSSP), and a 2mM Borate buffer bath. The biological materials that were utilized were samples of Synagis (Palivizumab) and strains of purified A2 Human Respiratory Syncytial Virus (RSV). The mechanical tools that were utilized in this experiment were a 24 slot centrifuge machine, some 250 mL Erlenmeyer flasks, a magnetic hot plate, some AmiconTM ultra centrifugal filter units, a 28 picosecond 532 nm PL 2230 Ekspla pulse laser, a 633 nm Newport red HeNe continuous laser, a photodector to detect the changes in the mV from the laser beam, a light filter wheel to adjust the intensity of the laser beam, mirrors and apertures to focus and align the beams, a 200 μm microcapillary, a Synergy 2 BioTek plate reader, a Malvern ZetaSizer Nano ZS DLS Machine, a 10K MWCO Dialysis Cassette, a JEOL JEM-2010 transmission electron microscope, a syringe pump, a variety of different sized pipets, an oscilloscope for data collection, and a computer with the MATLAB software for data collection.

IV. Synthesis of the 15 nm AuNPs

The Plech Turkevich method was utilized to synthesize the 15 nm AuNPs. The 15 nm AuNPs were used in order to conjugate with the Synagis (Palivizumab) antibodies to attach and conjugate the RSV virion samples. First, 98 mL of dH₂O and 1 mL of the 25 mM Tetrachloroauric (III) acid trihydrate were mixed inside a pre-cleaned 250 mL Erlenmeyer flask on a magnetic hot plate. The solution was mixed vigorously and heated to a boil. Next, 1 mL of the 112.2 mM Sodium Citrate tribasic dihydrate was injected into the flask using a 1000 μ L pipet. Finally, the flask was removed from the magnetic hot plate after a color change occurred in the flask, indicating that the reaction has been completed. After the process was completed, spectral absorbance of the 15 nm AuNP samples were measured by a Synergy 2 BioTek plate reader and their hydrodynamic size was measured and checked using a Malvern ZetaSizer Nano ZS DLS machine. This step was then repeated multiple times to create multiple batches for the different trials.

V. Conjugation of Antibodies and RSV with the AuNPs

The Synagis (Palivizumab) antibodies were conjugated with one batch of the 15 nm AuNPs. The antigen binding sites of the Synagis (Palivizumab) antibodies target and bind to the RSV surface F glycoproteins, allowing the RSV virions to be conjugated with the AuNPs. The DTSSP crosslinker was linked to the surface of the AuNP and links the Synagis (Palivizumab) antibodies to the AuNPs. During this step of the process, the amine-reactive N-hydroxysulfosuccinimide (sulfo-NHS) ester group at the two ends of the DTSSP reacts with the amine groups on the Synagis (Palivizumab) antibodies at pH 7-9, forming stable amide bonds. The DTSSP contains a disulfide bond in the center of the compound. (**Figure 3**). Through hydrolysis, the disulfide bond

is able to be split apart into two separate identical parts. After the sulfo-NHS-ester bonds react with the primary amine bonds in antibodies and bond together, the single sulfure bonds at the center of the DTSSP crosslinking reagent will form covalent bonds with the sulfurs on the surface of the AuNP.

Figure 2: Chemical Structure of a DTSSP crosslinking reagent

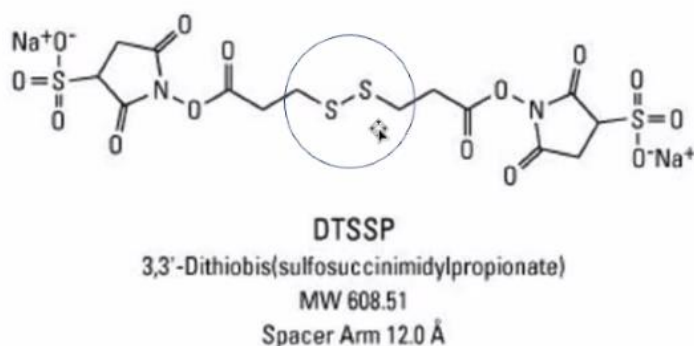


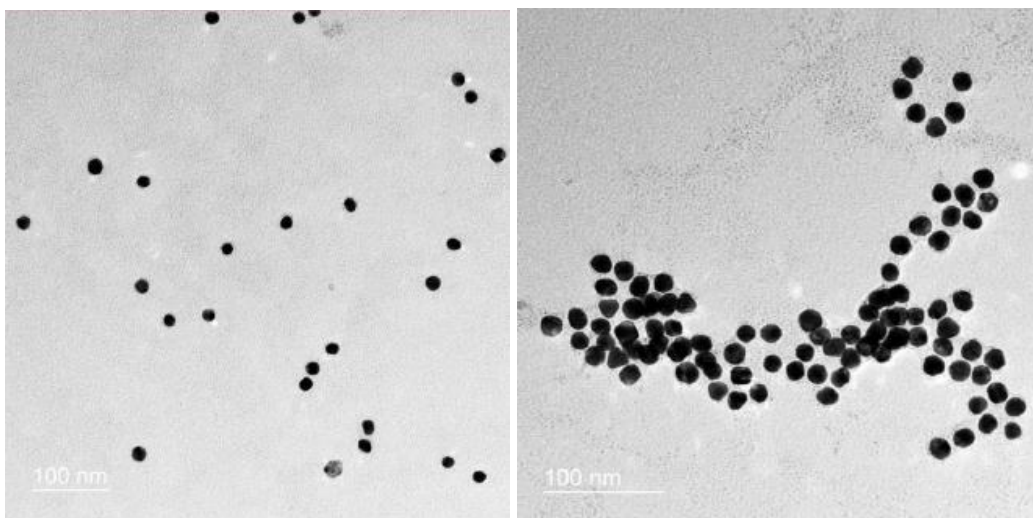
Image created by ThermoFisher Scientific and edited by the researcher

First, 1 mL of 15 nm AuNPs were washed by a high-speed centrifugal machine with 10,000 g for 25 minutes before being added back to the 2 mM borate buffer (pH = 8.5). Next, 5 mM of the DTSSP was added to the Synagis (Palivizumab) with a molar ratio of 125:1. Then, the DTSSP-Synagis solution was injected into a 10K MWCO Dialysis Cassette and dialyzed for 4 hours before being transported into 100 kDa AmiconTM centrifugal filters to remove and clean out the unlinked DTSSP. The resulting DTSSP-Synagis solution was then added to the 15 nm AuNPs in the 2 mM borate buffer. Finally, the solution was kept in an ice bath for 2 hours before getting washed by the centrifuge machine for a couple of times. The 15 nm AuNPs were now conjugated and linked together with the DTSSP-Synagis link, forming an AuNP-DTSSP-Synagis link. The

AuNP-DTSSP-Synagis was then stored in the 2 mM borate buffer at 4 °C. This process was repeated for two steps because one batch was utilized as the calibration control to determine the threshold for the single-AuNP counting mechanism, while the other batch was further conjugated with the purified RSV virus and utilized in the single-virion counting mechanism. One batch of the AuNP-DTSSP-Synagis solution was cleaned and prepared to be conjugated with the purified RSV strains. The purified RSV strains were incubated with the AuNP-DTSSP-Synagis in the 2 mM Borate buffer at room temperature. After 30 minutes, the solution was removed.

Figure 3 (Left): 15 nm AuNP-DTSSP-Synagis probes

Figure 4 (Right): RSV-conjugated 15 nm AuNP-DTSSP-Synagis probes



Both images taken using a Transmission Electron Microscopy at the University of Texas at Dallas

VI. Detection System Setup

The setup for the plasmonic nanobubble detection system consists of a 532 nm 28-picosecond pulse laser and a 633 nm red Helium Neon continuous laser that is aligned through the cross-section of a 200 μm microcapillary (**Figure 5**) and then focused into a photodetector using apertures and mirrors. The energy from the laser beams is collected using the photodetector and an oscilloscope (**Figure 6**).

Figure 5: Microcapillary alignment with the lasers

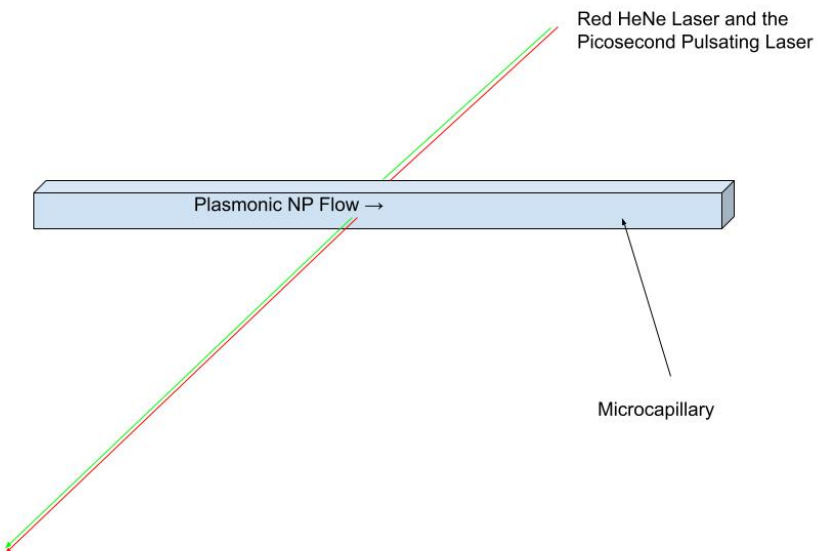
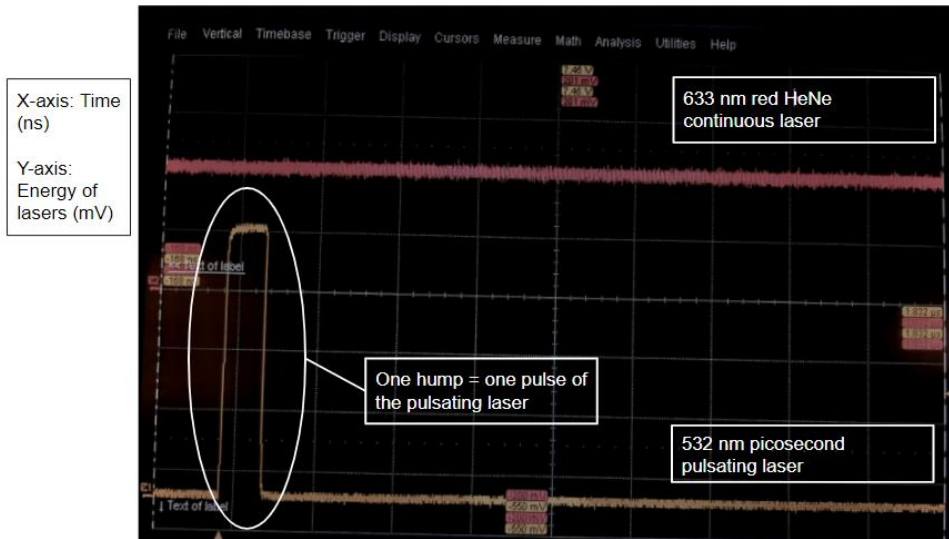


Figure 6: Oscilloscope



Both images were created and captured by the researcher respectively

A syringe pump and a syringe are attached to one end of the capillary. To start the machine, deionized UV water is added into the syringe and flushed through the microcapillary to clean out any debris from the system. Next, the picosecond laser's frequency was adjusted to 50 hertz. Then, the plasmonic nanoparticle solution is added into the syringe and pumped out the other side with a flow rate of 6 $\mu\text{L}/\text{minute}$. Finally, the data is recorded and collected on a file via the oscilloscope; the file can then be transported and stored onto a hard drive in a computer.

VII. Plasmonic Nanobubble Counting Mechanism

The plasmonic nanobubble detection and counting mechanism relies on a couple of key concepts: 1) The specific wavelength absorbance of 15 nm AuNPs, 2) the formation of nanobubbles, 3) light diffraction in nanobubbles, and 4) the counting mechanism. The reason why a 532 nm laser was utilized in this experiment was because the optimal light absorbance spectrum for 15 nm AuNPs is around 520-535 nm. This means that the AuNPs would have

absorbed the greatest amount of energy from lasers within that range, the plasmonic resonance. The laser pulses ensure that the AuNPs will not absorb too much energy and burn up the surrounding microcapillary tube. Through the properties of surface plasmon resonance, the electrons on the surface of the 15 nm AuNPs will start to oscillate between the poles of the nanoparticle when they absorb the 532 nm wavelength of light from the laser. The electron oscillations will in turn cause the AuNP to vibrate and generate lots of heat. The heat will then increase the temperature of the surrounding water, generating a nanobubble around the nanoparticle. The plasmonic nanobubbles referred to in this paper are small vapor bubbles that form when the water surrounding the AuNP gets heated up. While the picosecond laser is utilized in this experiment as a tool to energize the AuNPs, the 633 red HeNe continuous laser is utilized to detect the formation and the sizes of the nanobubbles generated. When a nanobubble is generated, it will diffract some of the light of the red HeNe laser beam (**Figure 7**), causing the mV value on the oscilloscope to dip and form a small parabola.

Figure 7: The red HeNe laser getting diffracted by the nanobubble

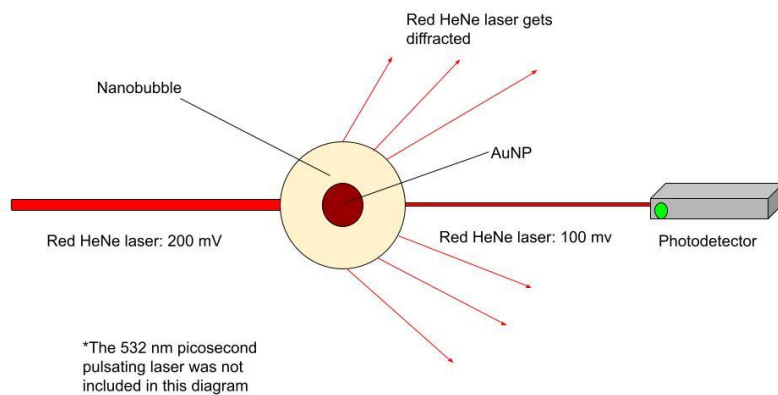


Image was created by the researcher

After every laser pulse, the mV value of the red HeNe laser beam is collected. If there is no dip of the red HeNe mV value, then a “F_{off}” signal is counted; if there is a dip of the red HeNe mV value, then a “F_{on}” signal is counted (**Figure 8**). The number of F_{on} signals counted is equal to how many AuNPs were detected in the whole solution.

Figure 8: Counting principal for the AuNPs

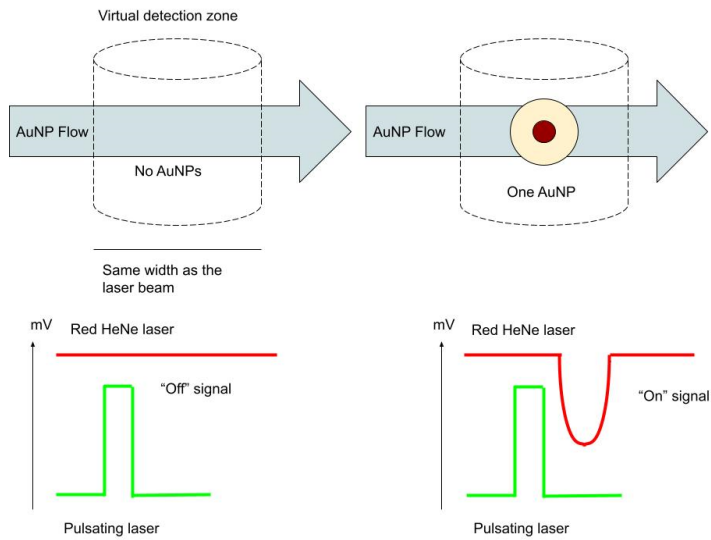


Image was created by the researcher

VIII. Single Virion Counting Mechanism

The basis for the single virion counting principal builds off of the key concepts discussed in **section VII**. As seen in **Figure 4**, after the Synagis antibodies on the AuNP attach onto the F glycoproteins, the AuNPs get aggregated together and form large clumps. When the large clumps pass through the laser's virtual detection zone, they are all energized by the laser all at once. This, in turn, will form larger bubbles compared to those formed by single AuNPs. The larger

bubbles formed by the RSV-conjugated AuNPs will diffract more of the laser beam light compared to the bubbles formed by the single unconjugated AuNPs (**Figure 9**).

Figure 9: Single AuNP detection vs single virion detection

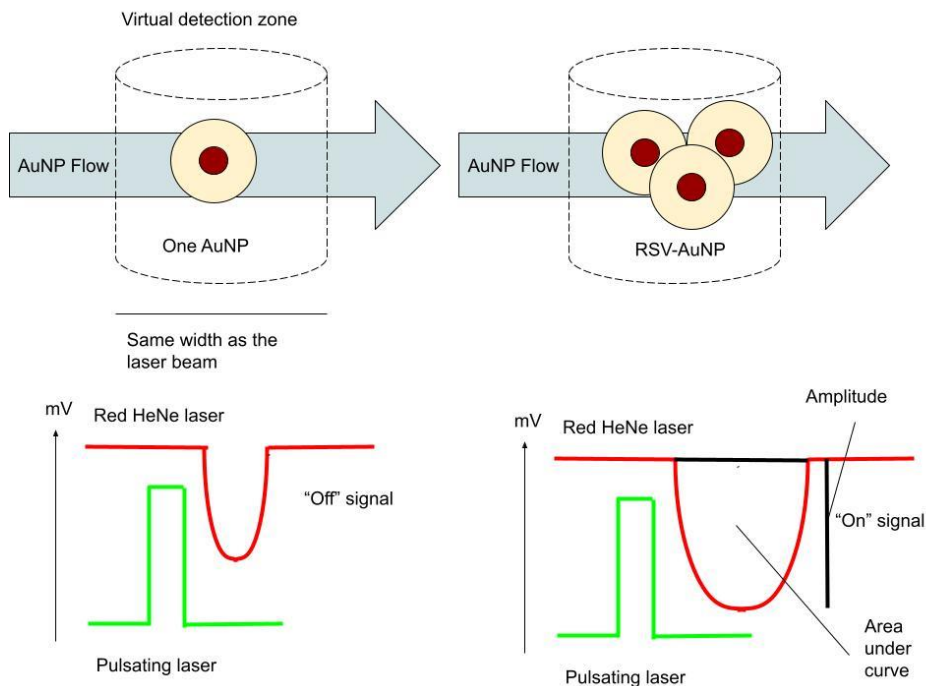


Image was created by the researcher

There is a larger dip for the RSV-conjugated AuNPs compared to the single AuNP detection because as the nanobubbles increase, more of the light energy from the Red HeNe laser will get refracted, indicating a larger dip in the energy (mV) detected by the photodetector. Additionally, the “ F_{off} ” and “ F_{on} ” signals were recalibrated and recalculated from the single AuNP detection to fit the RSV-conjugated AuNP detection. To do this, the thresholds were determined by using bivariate data plots to analyze the amplitudes (mV) and the area under the curve (AUC) for the two types of dips: unconjugated AuNP nanobubble dips and RSV-AuNP nanobubble dips. First,

the serial dilutions of the unconjugated AuNPs are used as the control group to calculate the thresholds. Next, the thresholds are determined by calculating the mean (μ) plus 5 standard deviations (σ), and since both the amplitudes and the AUC of the 15 nm AuNPs are normally distributed, the threshold values covered well over 99.99% of all amplitudes and AUCs from the control sample. Any amplitude and AUC that is lower than the threshold values will be counted as a “F_{off}” signal and, any that are higher than the threshold values will be counted as a “F_{on}” signal (**Figure 10**). Since the only signals that can possibly have higher AUC and amplitude values than the threshold values are the RSV-AuNP signals, the number of “F_{on}” signals is equal to the number of virions of RSV counted.

Figure 10: Threshold value determination

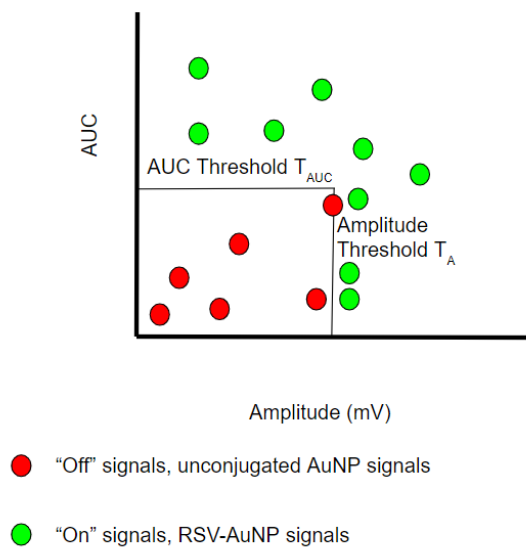


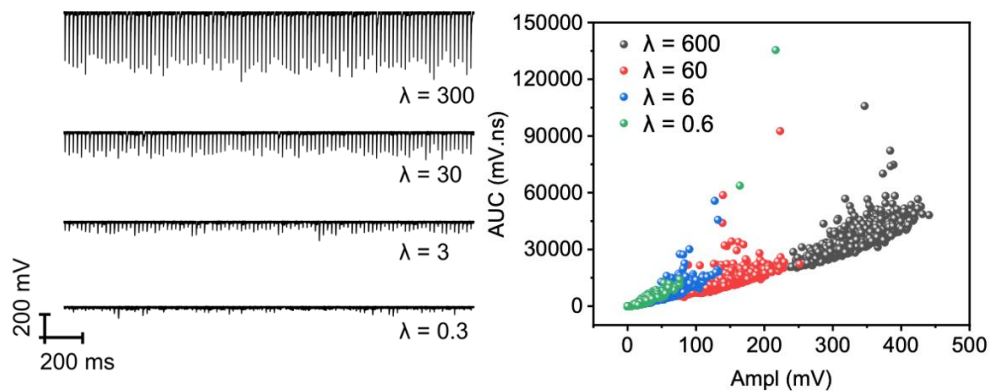
Image was created by the researcher

IX. Results and Conclusions

Starting with the single plasmonic nanobubble counting mechanism, the experiment used 6 different λ values (λ = number of estimated AuNPs per virtual detection zone): 0.3, 3, 30, 300 and 0.6, 6, 60, 600. The λ value is determined by $\lambda = -\ln(1 - F_{on}\%)$, $F_{on}\% = (F_{on}/F_{on}+F_{off}) * 100$. The size of the virtual detection zone is determined by $V = c/\lambda$, where c = concentration of NPs.

Figure 11 (Left): Raw data values for 100 pulses with λ between 0.3-300

Figure 12 (Right): Scatter plot for amplitude and AUC of AuNPs with λ between 0.6-600



Both images were created by the researcher

In **Figure 11**, each pulse shows a dip in the red HeNe mV on the oscilloscope. As λ increases, the more AuNPs are in the detection zone meaning that concentration has increased. This has the same effect as the RSV-conjugating AuNP signals as both increasing concentration and conjugation will increase λ . As λ increases, the amplitudes and AUC both increased proportionally. In **Figure 12**, the same experiment was conducted except λ was doubled for every value, and the amplitudes and AUC were extracted from the dips and plotted on a scatter

plot. Next, the single-virion counting mechanism was tested. A λ value of 60 was utilized for this experiment. First, 100 pulses were collected, and their amplitudes and AUCs were plotted on a scatter plot (**Figure 13**). The thresholds calculated were: $T_{AMP} = 225.65$ mV, $T_{AUC} = 137.13$.

Figure 13: Control sample threshold

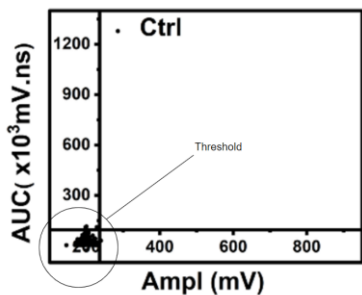
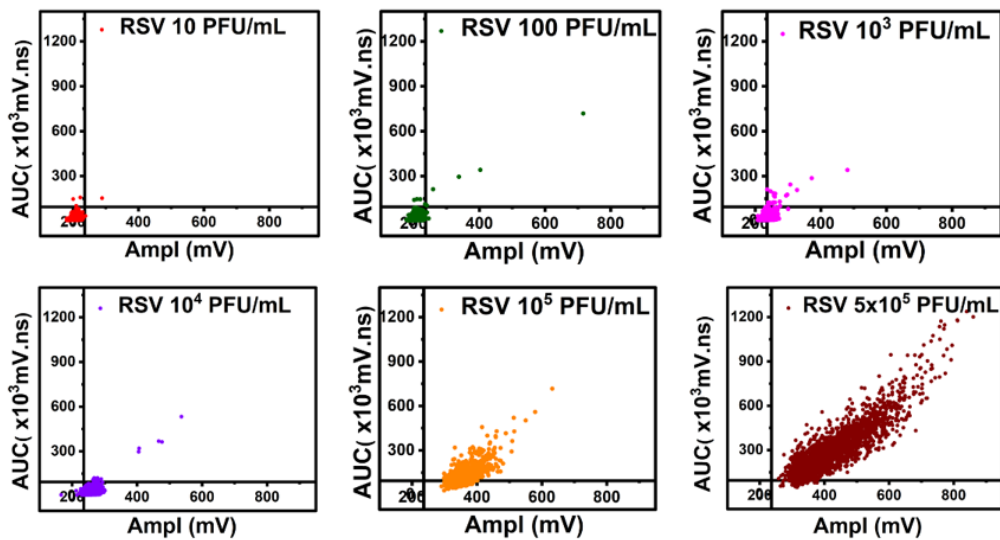


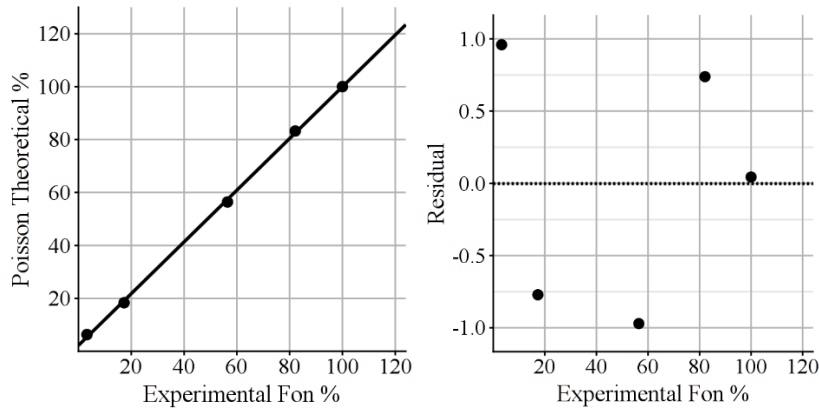
Figure 14: Single virion counting system



Both images were created by the researcher

As the virion concentration increases, the F_{on} number increases proportionally too. For example, when the virion sample was at 10 PFU/mL, there were only 3 total RSV virions in the entire sample. When the virion sample was increased to 100 PFU/mL, the system counted 10 total virions. When the virion sample was increased to 10^3 PFU/mL, the $F_{on}\%$ was 56.45% with 572 virions, meaning that there were more virions in the sample than free-floating AuNPs. When the virion sample was increased to 10^5 PFU/mL, the system determined that the $F_{on}\%$ of the viral sample was now 100%, meaning that every AuNP was attached to an RSV virion. The virion counting mechanism can be statistically cross-validated with Poisson statistics.

Figure 15: Poisson theoretical % vs experimental $F_{on}\%$



Both images were created by the researcher

Since there is a randomized residual plot, this means that the relationship between the Poisson theoretical % and the experimental $F_{on}\%$ is linear, and the r value for the scatter plot is 0.989. this shows that the relationship between the two variables is almost perfect. This indicates that there is little to no difference between the theoretical and observed values. The only concern for a slight error could be the 10 PFU/mL titer one as there was a slightly larger difference between

the Poisson estimate and the experimental data compared to the other titers. In conclusion, the machine was very effective in not only diagnosing patients, but also counting the number of virions in a fast and rapid way. On average, the test results were retrieved in around 7 to 8 minutes, faster than our current fastest diagnosis method by half the time while being almost 30% more accurate. Compared to our current medical standards of LAMP and PCR tests, this test is equally accurate while offering more sensitivity and versatility, all while costing significantly less.

X. Future Research and Applications

There is still much work to be done on this novel system, though. Today's experiment is only just the start to an innovative idea. For example, one of the main problems that needs to be answered is the issue of the viral load being too high in a sample. When the viral load exceeds well over 100% F_{on} , then the virion counting system won't effectively work because there will be multiple virions bonded to a cluster of AuNPs. The addition of an analog detection system would solve this issue; however, that would take more time and resources to develop. One major improvement would be the utilizing of a nanosecond laser as the excitation beam rather than a picosecond laser. This would greatly reduce the size and the cost of the laser, further reducing the costs. Finally, testing out different sizes of nanoparticles and concentrations to better optimize the aggregation properties of the AuNPs would make this method even more accurate and efficient.

XI. Acknowledgements

This project would not have been possible without the help of all the University of Dallas research team. My partner and I am forever grateful for their resources throughout this entire project.

XII. Work Cited

- Liu, Y., Ye, H., Huynh, H., Xie, C., Kang, P., Kahn, J. S., & Qin, Z. (2022). Digital plasmonic nanobubble detection for rapid and ultrasensitive virus diagnostics. *Nature communications*, 13(1), 1687. <https://doi.org/10.1038/s41467-022-29025-w>
- Fajnzylber, J., Regan, J., Coxen, K. *et al.* SARS-CoV-2 viral load is associated with increased disease severity and mortality. *Nat Commun* 11, 5493 (2020).
<https://doi.org/10.1038/s41467-020-19057-5>
- Surface Plasmon Resonance in Gold Nanoparticles: A Review - Iopscience.
<https://iopscience.iop.org/article/10.1088/1361-648X/aa60f3>.
- Li, Wanwan, and Xiaoyuan Chen. “Gold Nanoparticles for Photoacoustic Imaging.” Nanomedicine (London, England), U.S. National Library of Medicine, Jan. 2015,
<https://www.ncbi.nlm.nih.gov/pmc/articles/PMC4337958/>.
- Shkir, M., Khan, M. T., Ashraf, I. M., Almohammed, A., Dieguez, E., & AlFaify, S. (2019). High-performance visible light photodetectors based on inorganic CZT and InCZT single crystals. *Scientific reports*, 9(1), 12436. <https://doi.org/10.1038/s41598-019-48621-3>

- Nguyen, H. H., Park, J., Kang, S., & Kim, M. (2015). Surface plasmon resonance: a versatile technique for biosensor applications. *Sensors (Basel, Switzerland)*, 15(5), 10481–10510. <https://doi.org/10.3390/s150510481>